Electronic Supplementary Material (ESI) for ChemComm.

Supporting Information

MoS_2 Quantum Dots for electrocatalytic N_2 reduction

Yaojing Luo[#], Peng Shen[#], Xingchuan Li, Yali Guo, Ke Chu*

School of Materials Science and Engineering, Lanzhou Jiaotong University, Lanzhou 730070, China

*Corresponding author. E-mail address: chukelut@163.com (K. Chu)

[#] These authors contributed equally to this work.

Experimental Section

Synthesis of MoS_2 QDs

All the chemicals are of analytical grade and used as received. MoS_2 QDs were synthesized by a one-step microwave-assisted hydrothermal approach. Typically, 0.121 g of $Na_2MoO_4 \cdot 2H_2O$ were dispersed in 12.5 mL of deionized water followed by adjusting the pH to 6.5 with 0.1 M HCl. Then, 0.615 g of glutathione (GSH) was dissolved in 25 ml of deionized water. Afterwards, the above two solutions were mixed and sealed into a quartz tube, which were reacted for 30 min under microwave irradiation (2450 MHz). After cooling to room temperature, the mixture was collected by centrifugation, filtered through a 0.22 μm microporous membrane and further purified by dialyzing in deionized water. The solution was eventually concentrated by a rotatory evaporator and freeze-dried to obtain MoS_2 QDs.

Electrochemical experiments

Electrochemical measurements were performed under ambient conditions using a CHI-760E electrochemical workstation with a three-electrode cell. The Ag/AgCl (saturated KCl), graphite rod and catalyst on carbon cloth (CC) were used as reference, counter and working electrodes, respectively. The CC was pretreated by soaking it in 0.5 M H_2SO_4 for 12 h, and then washed with deionized water several times and dried at 60 ^oC for 24 h.All potentials were referenced to reversible hydrogen electrode (RHE) by following equation: E_{RHE} (V) = $E_{Ag/AgCl}$+0.197+0.059×pH. To prepare the working electrode, 1 mg of the catalyst was dispersed in 100 μL of ethyl alcohol containing 5 μL of Nafion (5 wt%) under sonication. The obtained homogeneous catalyst ink (20 μL) was dropped onto the pretreated CC electrode. The mass loading was 0.2 mg cm^{-2}. The NRR measurements were carried out using an H-type two-compartment electrochemical cell separated by a Nafion 211 membrane. The Nafion membrane was pretreated by heating it in 5% H_2O_2 aqueous solution at 80 °C for 1 h and then in deionized water at 80 °C for another 1 h. Before the NRR tests, all the feeding gases were purified through acid trap (0.05 M H_2SO_4) and alkaline trap (0.1 M KOH)) to remove any possible contaminants (NH_3 and NO_x). During the NRR

electrolysis, the purified N_2 gas was continuously purged into the cathodic chamber at a flow rate of 20 mL min^{-1}. After electrolysis, the produced NH_3 and possible N_2H_4 were quantitatively determined by the indophenol blue method[1], and approach of Watt and Chrisp[2], respectively. The detailed determination procedures are given in our previous publications [3-5].

Characterizations

Raman spectra were conducted on a JY-HR800 spectroscope. X-ray photoelectron spectroscopy (XPS) analysis was recorded on a PHI 5702 spectrometer. Transmission electron microscopy (TEM) and high-resolution transmission electron microscopy (HRTEM) were carried out on a Tecnai G^2 F20 microscope. Fluorescence spectra were recorded on an F-4700 fluorescence spectrophotometer. UV-vis absorbance measurements were performed using a MAPADA P5 spectrophotometer.

Calculation details

All spin-polarized density functional theory (DFT) calculations were performed using the Cambridge sequential total energy package (CASTEP). The exchange-correlation interactions were described by the Perdew−Burke−Ernzerhof (PBE) functional. Electronic energies were computed with the tolerance of 2×10^{-5} and total forces were converged to less than 0.05 eV/Å. The 4×4×1 Monkhorst-Pack mesh was used in Brillouin zone sampling. The kinetic cutoff energy for the plane wave basis was set at 500 eV. The MoS_2 nanocluster model derived from the layered MoS_2 is constructed to simulate the MoS_2 QDs. A vacuum region of 15 Å was used to separate adjacent slabs.

The adsorption energy (ΔE) is defined as [6]

$$\Delta E = E_{ads/slab} - E_{ads} - E_{slab} \quad (1)$$

where $E_{ads/slab}$, E_{ads} and E_{slab} are the total energies for adsorbed species on slab, adsorbed species and isolated slab, respectively.

The Gibbs free energy (ΔG, 298 K) of reaction steps is calculated by [6]:

$$\Delta G=\Delta E + \Delta ZPE - T\Delta S \quad (2)$$

where ΔE is the adsorption energy, ΔZPE is the zero point energy difference and $T\Delta S$

is the entropy difference between the gas phase and adsorbed state. The entropies of free gases were acquired from the NIST database.

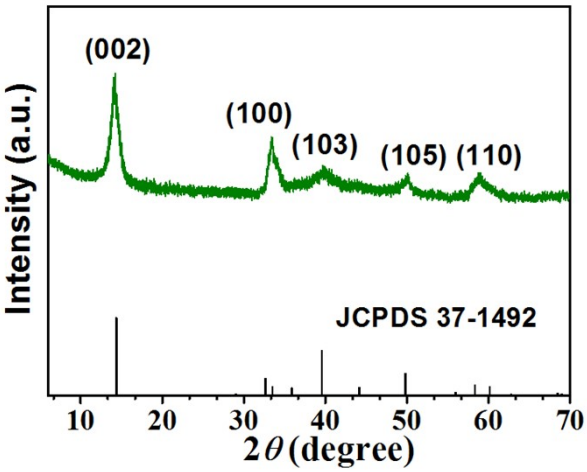

Fig. S1. XRD pattern of MoS_2 QDs.

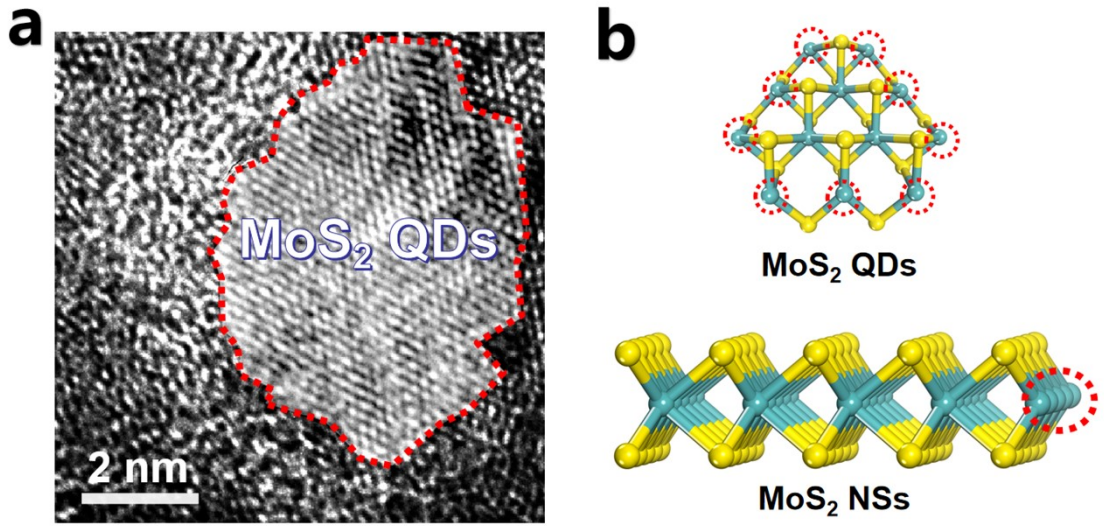

Fig. S2. (a) HRTEM image of MoS_2 QDs. (b) Atomic models of MoS_2 QDs and MoS_2 nanosheets (NSs), showing that MoS_2 QDs enable the exposure of more edge sites than MoS_2 nanosheets NSs.

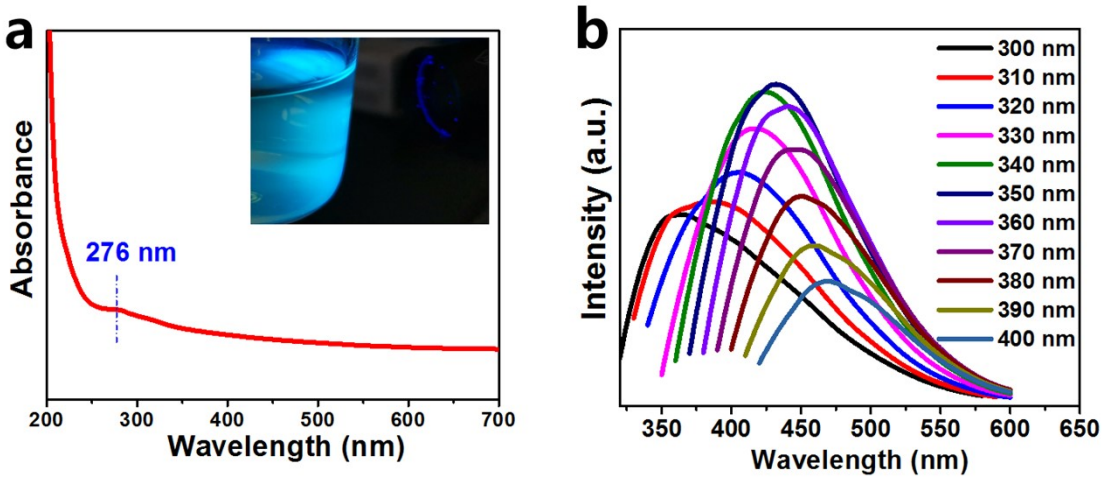

Fig. S3. (a) UV-vis spectra of MoS_2 QDs (Inset: digital photograph of MoS_2 QDs solution irradiated by UV light). (b) Photoluminescence emission spectra of MoS_2 QDs at the excitation wavelengths of 300-400 nm.

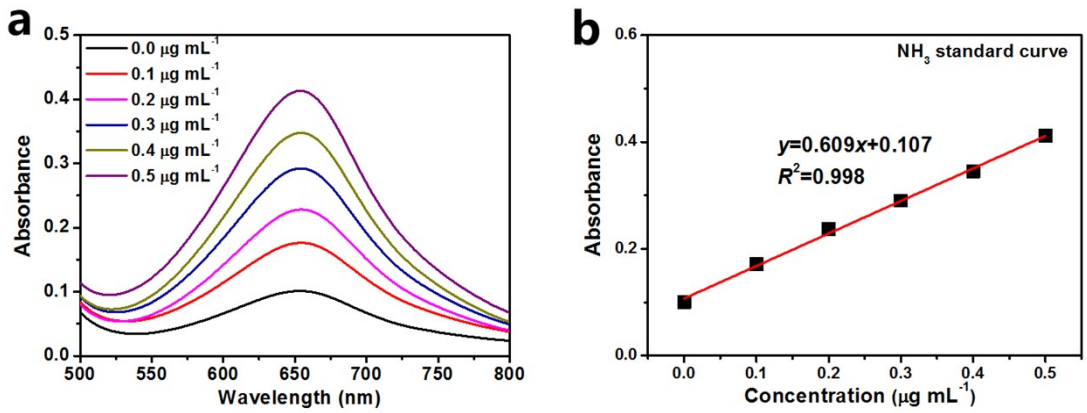

Fig. S4. (a) UV-Vis absorption spectra of indophenol assays with NH_4Cl after incubated for 2 h at ambient conditions. (b) Calibration curve used for calculation of NH_3 concentrations.

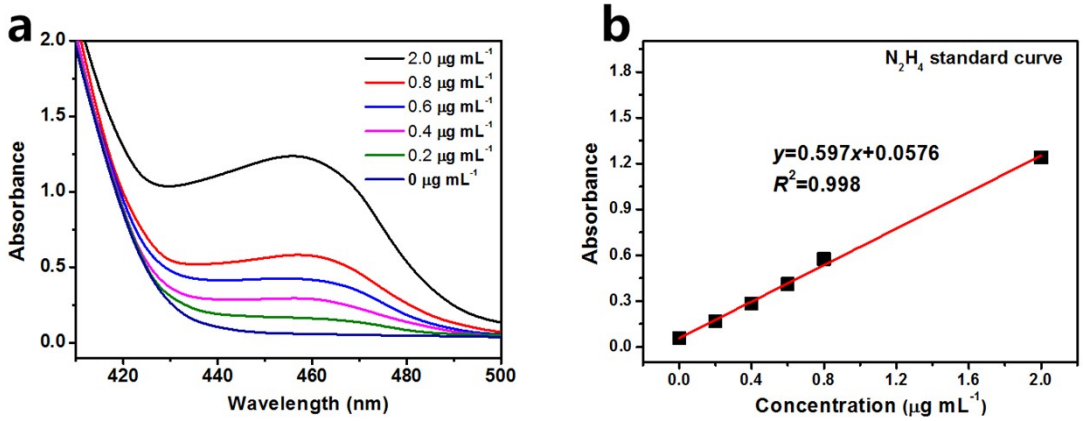

Fig. S5. (a) UV-vis absorption spectra of N_2H_4 assays after incubated for 20 min at ambient conditions. (b) Calibration curve used for calculation of N_2H_4 concentrations.

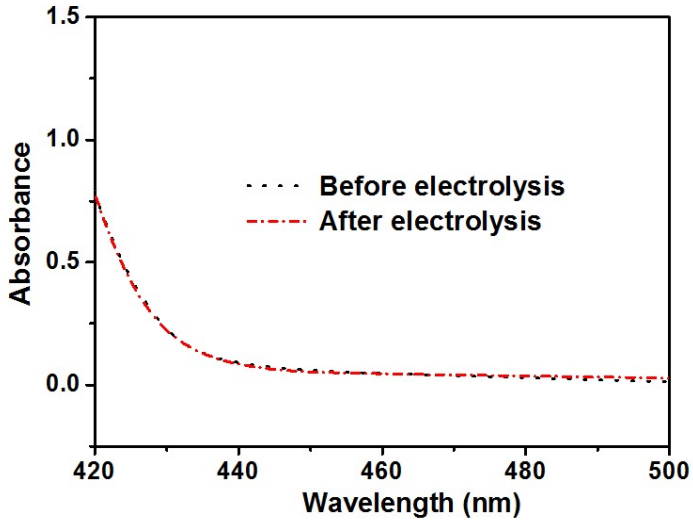

Fig. S6. UV-vis spectra of the electrolytes (stained with the chemical indicator based on the method of Watt and Chrisp) before and after 2 h of NRR electrolysis over MoS_2 QDs at -0.3 V.

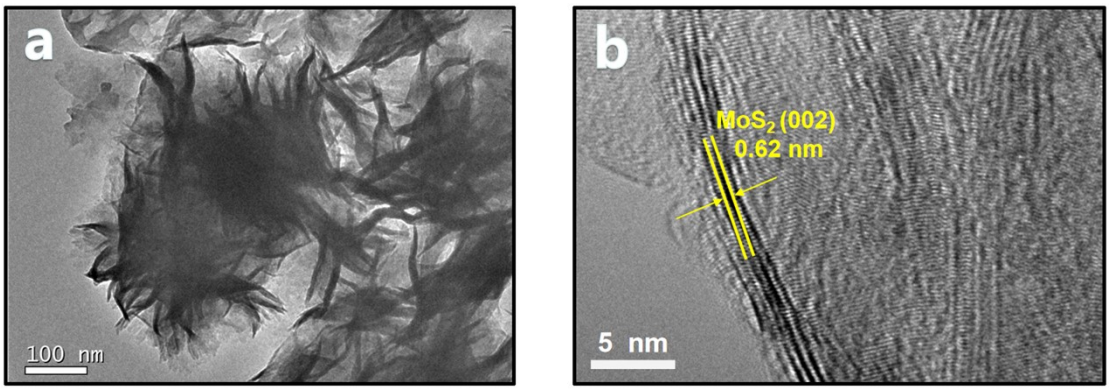

Fig. S7. (a) TEM and (b) HRTEM images of MoS_2 NSs. MoS_2 NSs were prepared by a hydrothermal method reported in our previous work[7].

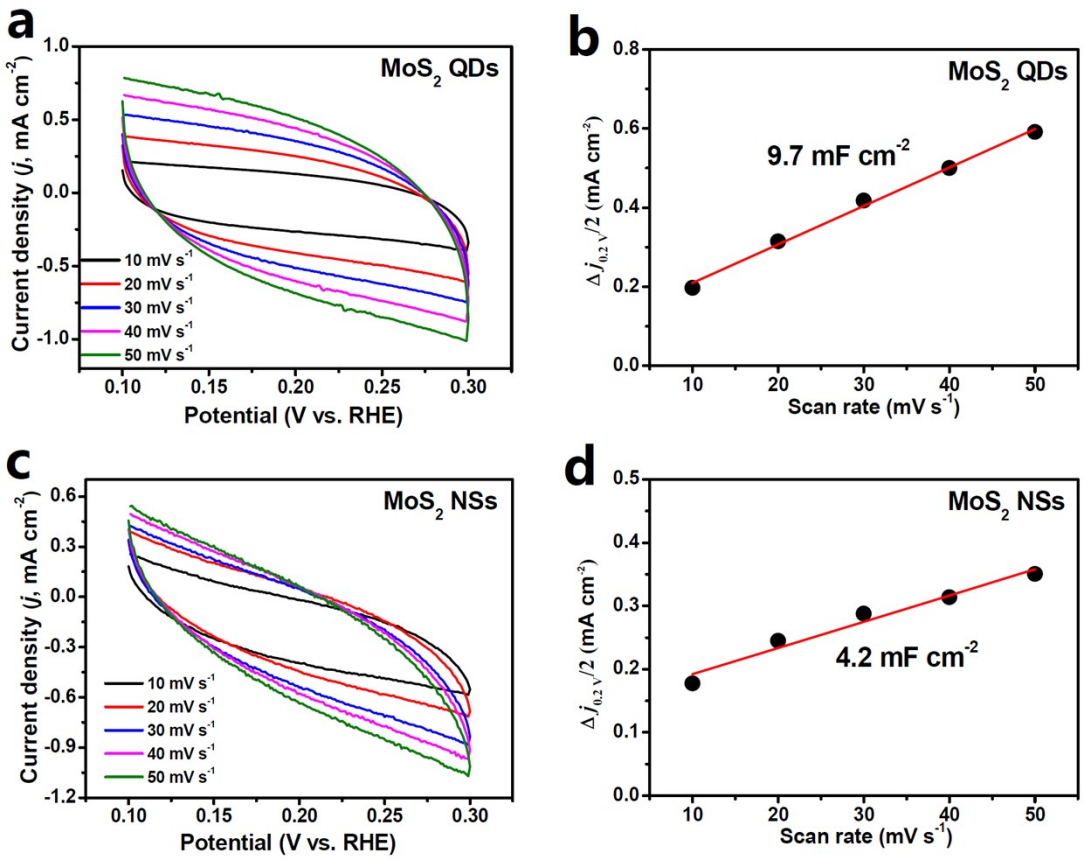

Fig. S8. Electrochemical double-layer capacitance (C_{dl}) measurements at different scanning rates of 10~50 mV s^{-1} for (a, b) MoS_2 QDs and (c, d) MoS_2 NSs.

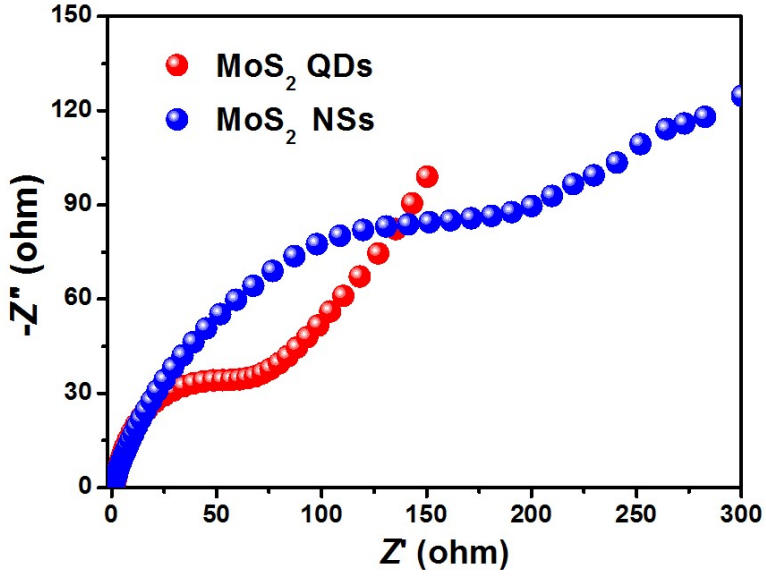

Fig. S9. Electrochemical impendence spectra of MoS_2 QDs and MoS_2 NSs.

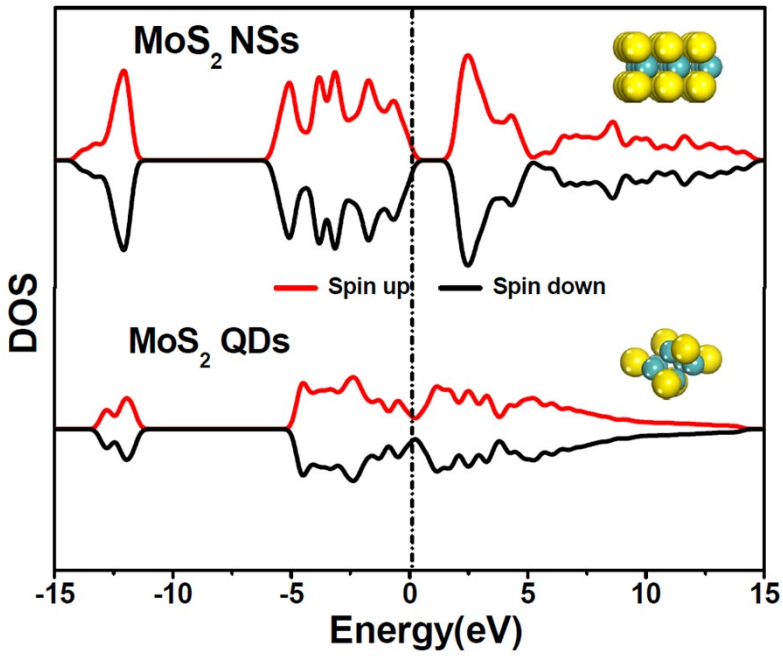

Fig. S10. DOS of MoS_2 QDs and MoS_2 NSs.

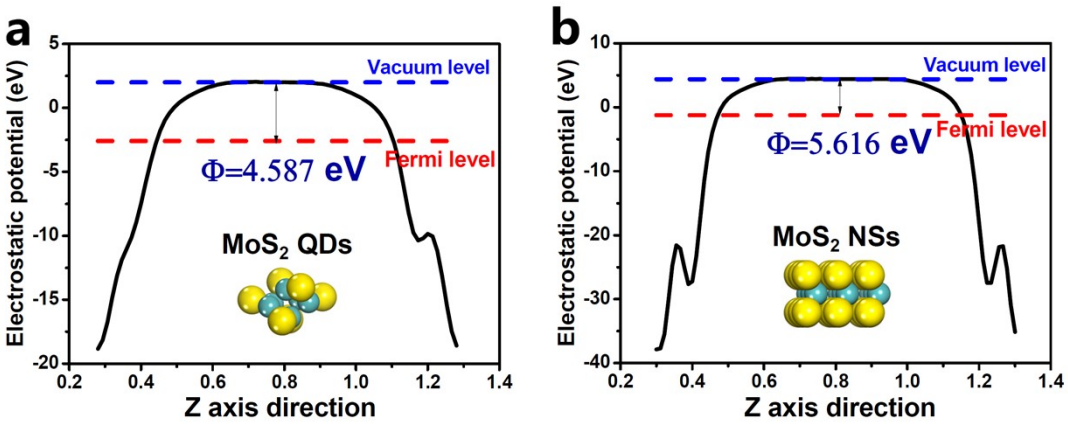

Fig. S11. Average potential profiles along c-axis direction for calculating the work functions of (a) MoS_2 QDs and (b) MoS_2 NSs.

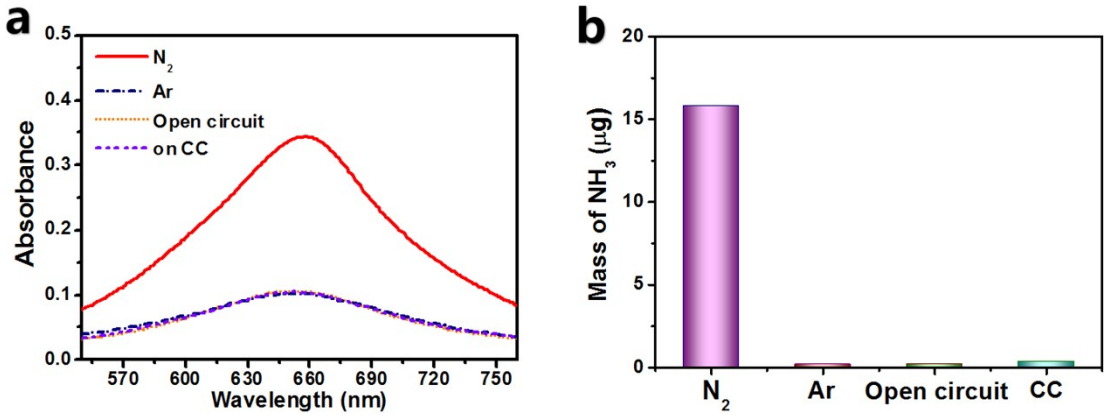

Fig. S12. (a) UV-vis absorption spectra of working electrolytes after 2 h of electrolysis in Ar-saturated solutions on MoS_2 QDs at -0.3 V, N_2-saturated solution on MoS_2 QDs at open circuit, and N_2-saturated solution on pristine CC at -0.3 V, and corresponding (b) Mass of produced NH_3.

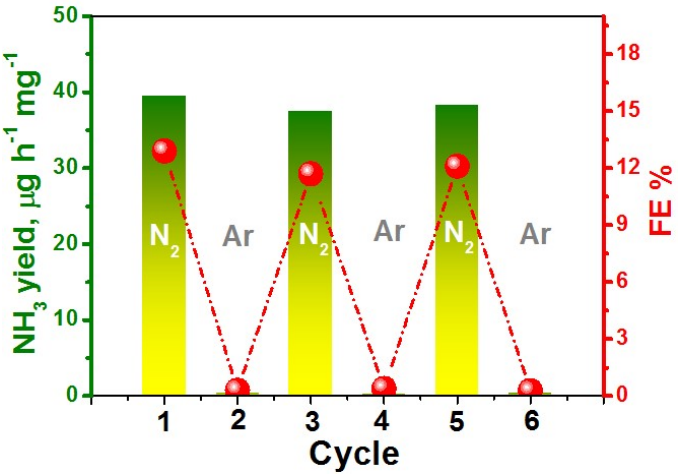

Fig. S13. Alternating cycling test in Ar- and N_2-saturated solution over MoS_2 QDs at -0.3 V.

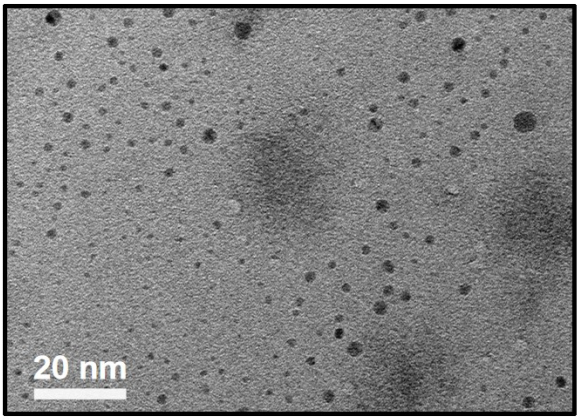

Fig. S14. Morphologies of MoS_2 QDs after stability test.

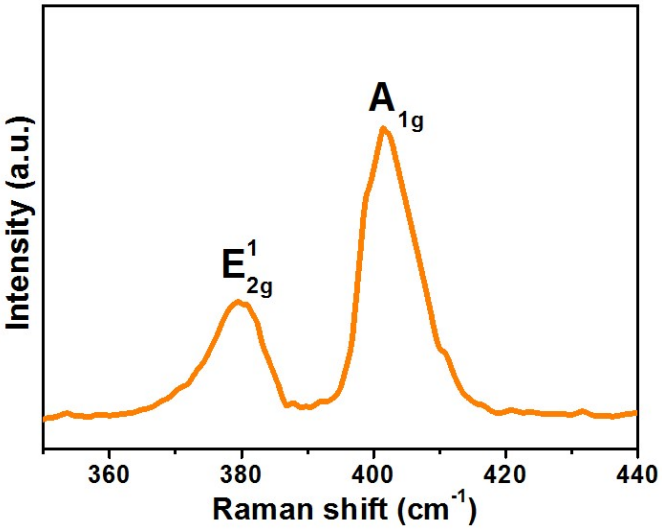

Fig. S15. Raman spectra of MoS_2 QDs after stability test.

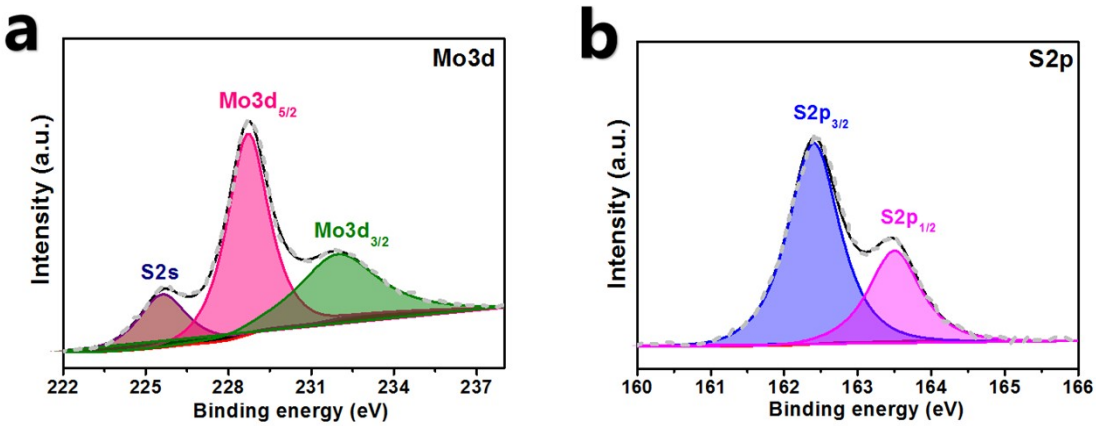

Fig. S16. XPS spectra of MoS_2 QDs after stability test: (a) Mo3d; (b) S2p.

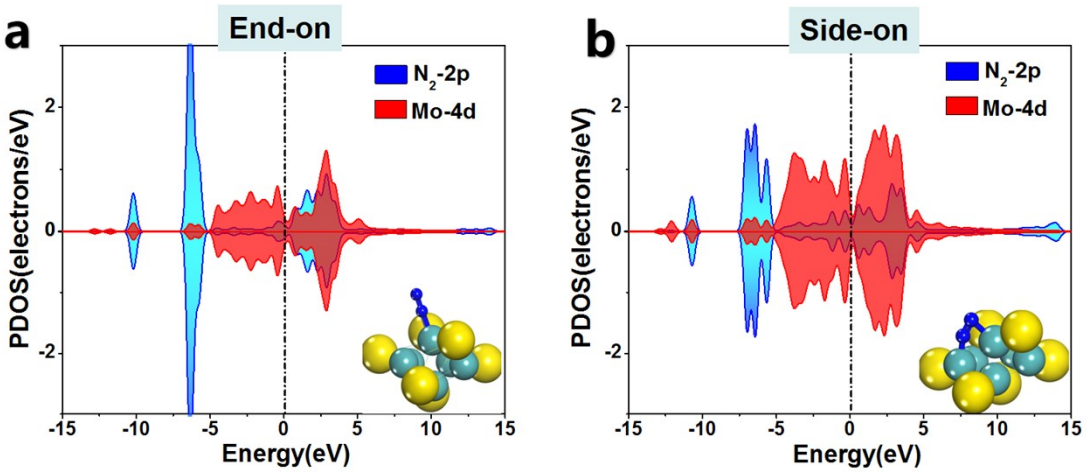

Fig. S17. PDOS of $*N_2$ on MoS_2 QDs via (a) end-on pattern and (b) side on pattern.

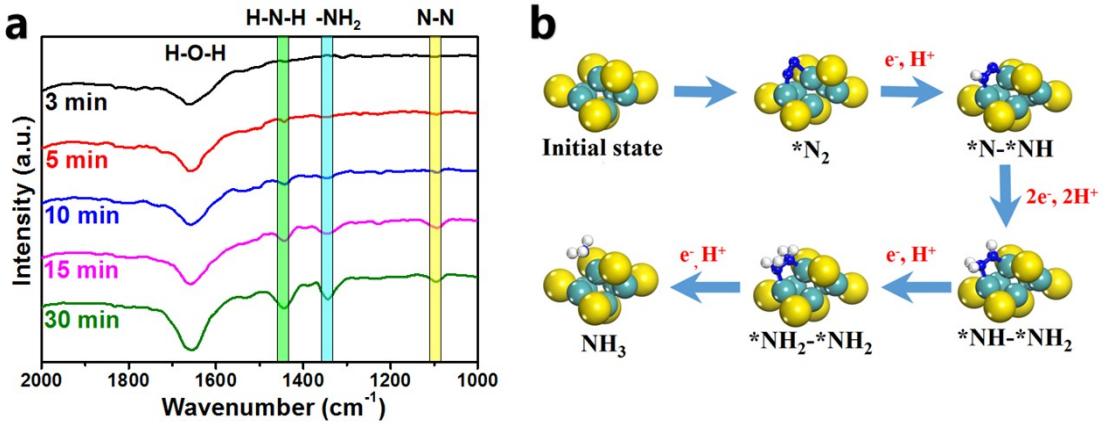

Fig. S18. (a) in-situ FT-IR spectra on MoS_2 QDs during the NRR electrocatalysis at various times (3-30 min) under -0.3 V. The in-situ FT-IR test follows the same procedure reported elsewhere[8]. (b) Proposed NRR associative pathway on MoS_2 QDs.

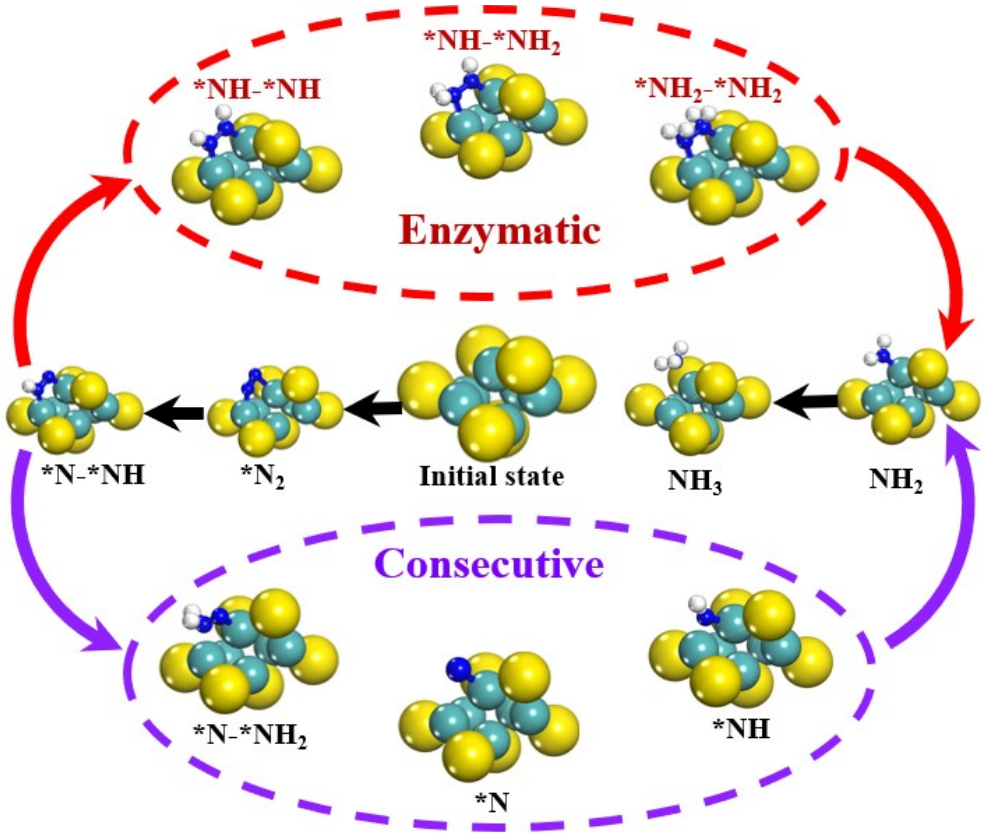

Fig. S19. Schematic of the enzymatic and consecutive NRR pathways on MoS_2 QDs and corresponding optimized structures of reaction intermediates.

Table S1. Comparison of the optimum NH_3 yield and Faradic efficiency (FE) for state-of-the-art NRR electrocatalysts at ambient conditions

Catalyst	Electrolyte	Potential (V vs RHE)	NH_3 yield rate	FE(%)	Ref.
Pd/C	0.1 M PBS	0.1	4.5 $\mu g\ h^{-1}\ mg^{-1}$	8.2	[9]
CoP hollow nanocage	1.0 M KOH	-0.4	10.78 $\mu g\ h^{-1}\ mg^{-1}$	7.36	[10]
Mo single atoms	0.1 M KOH	-0.3	34 $\mu g\ h^{-1}\ mg^{-1}$	14.6	[11]
MoO_2 with oxygen vacancies	0.1 M HCl	-0.15	12.2 $\mu g\ h^{-1}\ mg^{-1}$	8.2	[12]
Mosaic Bi nanosheets	0.1 M Na_2SO_4	-0.8	13.23 $\mu g\ h^{-1}\ mg^{-1}$	10.46	[13]
Mo_2C/C	0.5 M Li_2SO_4	-0.3	11.3 $\mu g\ h^{-1}\ mg^{-1}$	7.8	[14]
MoS_2 nanosheets	0.1 M Na_2SO_4	-0.5	8.08×10^{-11} mol $s^{-1}\ cm^{-2}$	1.17	[15]
Defect-rich MoS_2 nanoflower	0.1 M Na_2SO_4	-0.4	29.28 $\mu g\ h^{-1}\ mg^{-1}$	8.34	[16]
MoS_2 with Li-S Interactions	0.1 M Li_2SO_4	-0.2	43.4 $\mu g\ h^{-1}\ mg^{-1}$	9.81	[17]
MoS_2/RGO	0.1 M HCl	-0.45	24.82 $\mu g\ h^{-1}\ mg^{-1}$	4.58	[18]
Defective MoS_2	0.1 M Na_2SO_4	-0.5	29.55 $\mu g\ h^{-1}\ mg^{-1}$	4.58	[19]
V_S-MoS_2	0.1 M Na_2SO_4	-0.4	46.1×10^{-11} mol $s^{-1}\ cm^{-2}$	4.58	[20]
$Cu_{2-x}S$/MoS_2	0.1 M Na_2SO_4	-0.5	22.1 $\mu g\ h^{-1}\ mg^{-1}$	6.06	[21]
1T-MoS_2@Ti_3C_2	0.1 M HCl	-0.3	30.33 $\mu g\ h^{-1}\ mg^{-1}$	10.94	[22]
MoS_2/C_3N_4	0.1 M $LiClO_4$	-0.3	18.5 $\mu g\ h^{-1}\ mg^{-1}$	17.8	[7]
MoS_2 nanodots/RGO	0.1 M Na_2SO_4	-0.75	16.41 $\mu g\ h^{-1}\ mg^{-1}$	27.93	[23]
MoS_2 QDs	**0.5 M $LiClO_4$**	**-0.3**	**39.6 $\mu g\ h^{-1}\ mg^{-1}$**	**12.9**	**This wok**

Supplementary references

[1]. D. Zhu, L. Zhang, R. E. Ruther and R. J. Hamers, *Nat. Mater.*, 2013, **12**, 836.

[2]. G. W. Watt and J. D. Chrisp, *Anal. Chem.*, 1952, **24**, 2006-2008.

[3]. J. Wang, H. Nan, Y. Tian and K. Chu, *ACS Sustain. Chem. Eng.*, 2020, **8**, 12733-12740.

[4]. Y. Liu, Y. Luo, Q. Li, J. Wang and K. Chu, *Chem. Commun.*, 2020, **56**, 10227-10230.

[5]. Q. Li, Y. Cheng, X. Li, Y. Guo and K. Chu, *Chem. Commun.*, 2020, **56**, 13009-13012.

[6]. A. A. Peterson, *Energy Environ. Sci.*, 2010, **3**, 1311-1315.

[7]. K. Chu, Y. P. Liu, Y. B. Li, Y. L. Guo and Y. Tian, *ACS Appl. Mater. Inter.*, 2020, **12**, 7081-7090.

[8]. R. Hao, W. Sun, Q. Liu, X. Liu, J. Chen, X. Lv, W. Li, Y. p. Liu and Z. Shen, *Small*, 2020, **16**, 2000015.

[9]. J. Wang, L. Yu, L. Hu, G. Chen, H. Xin and X. Feng, *Nat. Commun.*, 2018, **9**, 1795.

[10]. W. Guo, Z. Liang, J. Zhao, B. Zhu, K. Cai, R. Zou and Q. Xu, *Small Methods*, 2018, **2**, 1800204.

[11]. L. Han, X. Liu, J. Chen, R. Lin, H. Liu, F. Lu, S. Bak, Z. Liang, S. Zhao and E. Stavitski, *Angew. Chem. Int. Edit.*, 2018, **58**, 2321-2325.

[12]. G. Zhang, Q. Ji, K. Zhang, Y. Chen, Z. Li, H. Liu, J. Li and J. Qu, *Nano Energy*, 2019, **59**, 10-16.

[13]. L. Li, C. Tang, B. Xia, H. Jin, Y. Zheng and S.-Z. Qiao, *ACS Catal.*, 2019, **9**, 2902-2908.

[14]. H. Cheng, L. X. Ding, G. F. Chen, L. Zhang, J. Xue and H. Wang, *Adv. Mater.*, 2018, **30**, 1803694.

[15]. L. Zhang, X. Ji, X. Ren, Y. Ma, X. Shi, Z. Tian, A. M. Asiri, L. Chen, B. Tang and X. Sun, *Adv. Mater.*, 2018, **30**, 1800191.

[16]. X. Li, T. Li, Y. Ma, Q. Wei, W. Qiu, H. Guo, X. Shi, P. Zhang, A. M. Asiri and L. Chen, *Adv. Energy. Mater.*, 2018, **8**, 1801357.

[17]. Y. Liu, M. Han, Q. Xiong, S. Zhang, C. Zhao, W. Gong, G. Wang, H. Zhang and H. Zhao, *Adv. Energy. Mater.*, 2019, **9**, 1803935.

[18]. X. Li, X. Ren, X. Liu, J. Zhao, X. Sun, Y. Zhang, X. Kuang, T. Yan, Q. Wei and D. Wu, *J. Mater. Chem. A*, 2019, **7**, 2524-2528.

[19]. B. Liu, C. Ma, D. Liu and S. Yan, *ChemElectroChem*, 2021, DOI: 10.1002/celc.202100534.

[20]. C. Ma, N. Zhai, B. Liu and S. Yan, *Electrochim. Acta*, 2021, **370**.

[21]. T. Jiang, L. Li, L. Li, Y. Liu, D. Zhang, D. Zhang, H. Li, B. Mao and W. Shi, *Chem. Eng. J.*, 2021, **426**.

[22]. X. Xu, B. Sun, Z. Liang, H. Cui and J. Tian, *ACS Appl. Mater. Inter.*, 2020, **12**, 26060-26067.

[23]. Y. Liu, W. Wang, S. Zhang, W. Li, G. Wang, Y. Zhang, M. Han and H. Zhang, *ACS Sustain. Chem. Eng.*, 2020, **8**, 2320-2326.